cancers

MDPI

Article

A Novel Framework for the Optimization of Simultaneous ThermoBrachyTherapy

Ioannis Androulakis [1,*], Rob M. C. Mestrom [2], Miranda E. M. C. Christianen [1], Inger-Karine K. Kolkman-Deurloo [1] and Gerard C. van Rhoon [1,3,*]

1 Department of Radiotherapy, Erasmus MC Cancer Institute, University Medical Center Rotterdam, 3015 Rotterdam, The Netherlands; m.christianen@erasmusmc.nl (M.E.M.C.C.); i.kolkman-deurloo@erasmusmc.nl (I.-K.K.K.-D.)
2 Department of Electrical Engineering, Eindhoven University of Technology, 5600 Eindhoven, The Netherlands; r.m.c.mestrom@tue.nl
3 Department of Radiation Science and Technology, Delft University of Technology, 2629 Delft, The Netherlands
* Correspondence: i.androulakis@erasmusmc.nl (I.A.); g.c.vanrhoon@erasmusmc.nl (G.C.v.R.)

Simple Summary: ThermoBrachyTherapy, a combination therapy where radiation and heat are simultaneously applied using needle-shaped applicators from within the target, is a potentially very effective treatment for prostate cancer. When radiation and thermal therapies are applied, the dose coverage of each treatment is preplanned without considering the combined effect of the two dose distributions. In this study, we propose a method to automatically plan the thermal dose in such a treatment, based on the combined effect with the radiation. Furthermore, we apply the method on 10 patients and compare the treatment to a brachytherapy-only treatment plan. In this way, we show that, with properly optimized ThermoBrachyTherapy, we can provide equivalent combined dose coverages to the prostate, while reducing the dose delivered to critical organs surrounding the prostate, which might translate to reduced toxicity of the treatment.

Abstract: In high-dose-rate brachytherapy (HDR-BT) for prostate cancer treatment, interstitial hyperthermia (IHT) is applied to sensitize the tumor to the radiation (RT) dose, aiming at a more efficient treatment. Simultaneous application of HDR-BT and IHT is anticipated to provide maximum radiosensitization of the tumor. With this rationale, the ThermoBrachyTherapy applicators have been designed and developed, enabling simultaneous irradiation and heating. In this research, we present a method to optimize the three-dimensional temperature distribution for simultaneous HDR-BT and IHT based on the resulting equivalent physical dose (EQD_{phys}) of the combined treatment. First, the temperature resulting from each electrode is precomputed. Then, for a given set of electrode settings and a precomputed radiation dose, the EQD_{phys} is calculated based on the temperature-dependent linear-quadratic model. Finally, the optimum set of electrode settings is found through an optimization algorithm. The method is applied on implant geometries and anatomical data of 10 previously irradiated patients, using reported thermoradiobiological parameters and physical doses. We found that an equal equivalent dose coverage of the target can be achieved with a physical RT dose reduction of 20% together with a significantly lower EQD_{phys} to the organs at risk (p-value < 0.001), even in the least favorable scenarios. As a result, simultaneous ThermoBrachyTherapy could lead to a relevant therapeutic benefit for patients with prostate cancer.

Keywords: hyperthermia; induced; brachytherapy; prostatic neoplasms; interstitial hyperthermia; treatment plan optimization; prostate; thermoradiotherapy; linear quadratic model; biological modeling

Citation: Androulakis, I.; Mestrom, R.M.C.; Christianen, M.E.M.C.; Kolkman-Deurloo, I.-K.K.; van Rhoon, G.C. A Novel Framework for the Optimization of Simultaneous ThermoBrachyTherapy. *Cancers* **2022**, *14*, 1425. https://doi.org/10.3390/cancers14061425

Academic Editor: David Wong

Received: 30 January 2022
Accepted: 10 March 2022
Published: 10 March 2022

1. Introduction

High-dose-rate brachytherapy (HDR-BT) is a well-established treatment option in localized prostate cancer treatment [1]. Radiobiological clinical data have shown that prostate

cancer, in contrast to most tumor sites, has a very low α/β ratio (α/β = 0.9–2.2 Gy) [2]. This is a value very close to or lower than the α/β of nearby organs at risk (OAR), with the urethra estimated at an α/β = 0.5–1 Gy [3] and the rectum estimated at an α/β = 1.6–3.1 Gy [4], depending on the considered toxicity endpoint. This very low α/β ratio is the reason that radiotherapy for prostate cancer is aimed towards hypofractionation, with extensive use of HDR-BT as a boost to external beam radiation therapy (EBRT) or even as a standalone therapy (monotherapy) [5,6].

In HDR-BT monotherapy for prostate cancer, several clinical trials have shown that even ultrahypofractionated treatments of 2–4 fractions lead to excellent overall disease-free survival in low-risk and favorable intermediate-risk cancer patients [6–8]. On the other hand, the treatments are still linked with genitourinary and gastrointestinal toxicities [9]. Moreover, further reduction to a single fraction treatment has shown very poor results in multiple studies, with the reasons for those poor results not yet clear. Furthermore, ultrahypofractionated HDR-BT monotherapy is currently not recommended in higher-risk patients [10,11].

The abovementioned drawbacks could be overcome if the treatment could further escalate the radiation dose in the prostate without affecting the OAR, or if the same dose could be reached in the prostate with a reduced dose in the OAR. A way to achieve this could be by selective target radiosensitization. One of the most potent sensitizers to radiation is hyperthermia [12,13]. It has also been shown in clinical data that hyperthermia reduces the α/β of tumors [14] and, hence, makes the tumors more favorable to hypofractionation. This is also evident in multiple in vitro experiments on specific prostate cancer cell lines [15–17]. Other than that, the ability of hyperthermia to increase perfusion, increase reoxygenation, and overcome radiation-resistant hypoxia [18] could enable a reinvestigation of single fraction treatments, since the lack of reoxygenation and hypoxic cells are presumed to be a possible cause of failure, according to Morton and Hoskin [19].

Together with HDR-BT, interstitial hyperthermia (IHT) can be used to sensitize the target [20]. This is especially convenient if the same catheters used for the HDR-BT treatment can also be used for the IHT application. IHT has been applied in various early clinical trials [21,22] and, lately, in a phase II clinical trial ongoing for salvage prostate cancer treatment [23], where three fractions of IHT (1 h at 40–43 °C) followed by 10 Gy HDR-BT were applied over three weeks.

Historical biological research has clearly shown that thermal radiosensitization depends on the time interval between radiation and hyperthermia, with the highest radiosensitization reached at simultaneous (i.e., radiation during hyperthermia) application of the two modalities [13,24]. Based on this rationale, we have developed novel Thermo-Brachytherapy (TBT) applicators that enable the simultaneous application of HDR-BT and capacitive coupled radiofrequency (CC-RF) interstitial heating [25]. The improved temperature-related technical characteristics of these applicators are described in our earlier publication [25].

The challenge in simultaneous thermal radiosensitization is that, according to Overgaard [26], normal tissue might be sensitized as much as the target tissue. Hence, in order to reach a therapeutic benefit with simultaneous application of the two modalities, both treatment modalities need to be confined to the target as much as possible [27]. In prostate cancer treatment, this is a challenging task, with OAR very close to (rectum, bladder) or in direct contact with (urethra) the target volume. Therefore, very precise treatment plan optimization is needed to reach a therapeutic benefit, taking into account the combined effect of both hyperthermia and radiation.

In recent years, substantial progress has been made in theoretical modeling to calculate and quantify the combined effect of radiation and hyperthermia [28–31]. Most notably, this has resulted in the temperature-dependent linear-quadratic (TDLQ) model [29] and its extended version, including direct temperature-induced cytotoxicity [30]. While these models have been used to evaluate existing treatment plans retrospectively, there has been

no attempt for pretreatment plan optimization based on the combined effect of radiation and hyperthermia.

In general, research on IHT treatment plan (IHT-TP) optimization is limited and rarely applied in clinical practice [20]. In [32], Chen et al. proposed an automated optimization algorithm for ultrasound-based IHT-TP. In [33], Salgaonkar et al. validated temperature superpositioning for faster optimization of ultrasound-based IHT-TP. In [34], Kok et al. proposed a framework for fast automated temperature optimization using basic temperature-based objective functions that can also be applied on CC-RF IHT. In [35], we validated a highly accurate fast calculation method for the power deposition of the TBT applicators. The next step in producing fast IHT-TP is to automate the treatment planning process.

This study presents the framework to optimize the IHT-TP parameters based on the equivalent RT dose resulting from the TDLQ model. This optimization framework is applied on real anatomical and implant data from 10 patients. The results demonstrate that, under clinically realistic circumstances, HDR-BT combined with simultaneous IHT using the TBT applicators has the potential to lead to a relevant therapeutic benefit in terms of OAR sparing or escalation of the equivalent physical dose.

2. Materials and Methods

2.1. Overview of Optimization Framework

In the following paragraphs, we detail all steps that constitute the optimization framework (Figure 1). To reach the optimal thermoradiobiological TBT plan, first, the planning CT images (Figure 1 Item 1) are used to create the patient tissue model (Figure 1 Item 2). The position of the TBT applicators is reconstructed, and the electromagnetic (EM) fields and temperature distributions are precomputed per electrode (Figure 1 Items 3 and 4). The dwell times and dwell positions, defining the physical radiation dose, are optimized autonomously using the standard clinical HDR-BT protocol and workflow (Figure 1 Item 5). The IHT-TP parameters are then optimized based on the combined effect of the temperature distribution and the radiation distribution (Figure 1 Item 8). To evaluate the combined effect in terms of equivalent physical dose (EQD_{phys}), the TDLQ model is applied (Figure 1 Item 6) with thermoradiobiological parameters from the literature. The optimization uses the standard clinical objectives and constraints as applied in the HDR-BT-only plans (Figure 1 Item 7).

2.2. Patient Anatomy Modeling

The patient tissues are modeled (Figure 1 Item 2) using information derived from computed tomography (CT) images taken as for HDR-BT planning (Figure 1 Item 1), with the dual function TBT applicators implanted into the patient. Prostate, urethra, rectum, bladder, bone, fat, muscle, and air volumes are distinguished. Prostate, urethra, rectum, and bladder volumes are defined by manual segmentation by an expert radiotherapy technologist using Oncentra® Brachy (Elekta Brachytherapy Solutions, Veenendaal, The Netherlands), and approved by a radiation oncologist. For the other tissues, an automated workflow, based on thresholding, developed for clinical deep hyperthermia treatment planning is used (MIM Software, Cleveland, OH, USA). An example CT image with implanted afterloading catheters instead of TBT applicators can be seen in Figure 2a. The corresponding tissue model on the same slice can be seen in Figure 2b. The TBT applicator visualization and positioning are expected to be identical to the afterloading catheters used in standard HDR-BT treatment.

2.3. TBT Applicator Modeling, Positioning, and E-Field Calculation

Each TBT applicator consists of two 20-mm-long cylindrical electrodes with a 5-mm separation deposited on a needle-shaped flexible polyoxymethylene afterloading catheter and coated with a thin Parylene C coating. The two electrodes are connected to a power source through two feeding lines running parallel to the catheter up to the proximal end of

the applicator. A detailed description of the applicator can be found in [25]. In the patient model, the TBT applicators are located and reconstructed as shown in the planning CT images (Figure 2c).

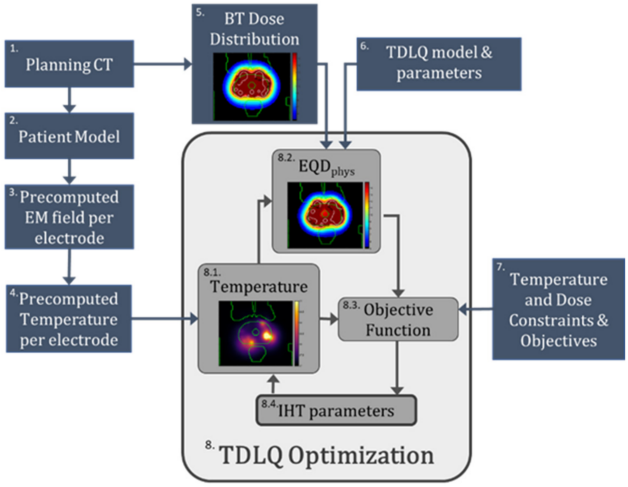

Figure 1. Graphical summary of the proposed optimization framework. 1. The planning CT is the initial input of the process. 2. The patient model is generated. 3. The EM field per electrode is precalculated. 4. The temperature distribution per electrode is precalculated. 5. The BT dose distribution is imported from the BT treatment planning software. 6. The TDLQ model is used for the calculation of the combined effect. 7. Both temperature and dose constraints and objectives are used for the optimization process. 8. The TDLQ optimization process optimizes the IHT parameters (8.4) that generate a temperature distribution (8.1) from which an EQD_{phys} distribution is generated (8.2). This EQD_{phys} distribution is used to compute the objective function, which needs to be minimized (8.3).

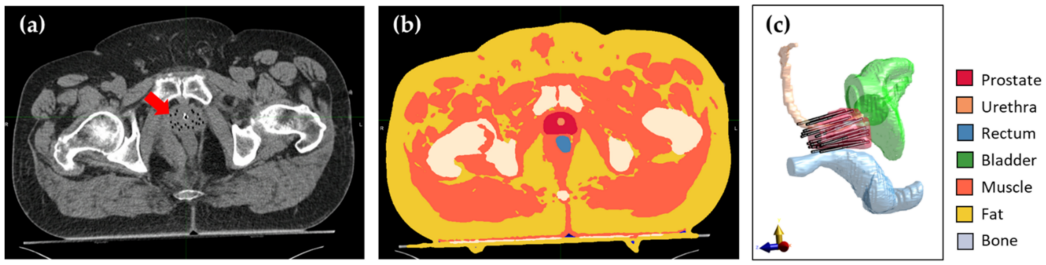

Figure 2. (**a**) Axial CT slice showing the anatomy of a patient with afterloading catheters (visible as black dots indicated by the arrow) inserted in the prostate. (**b**) Same axial slice of the resulting patient model after segmentation of all tissues. (**c**) Lateral 3D view of the prostate, OAR, and simulated TBT applicators in the same patient.

The electric field (E-field) is calculated for each electrode i as described in [35], using a finite element method solver for the electroquasistatic approximation [36]:

$$\nabla \cdot (\sigma + j2\pi f\varepsilon)\nabla \mathrm{V}_i = 0\,, \tag{1a}$$

$$E_i = -\nabla \mathrm{V_i} \tag{1b}$$

where σ is the electrical conductivity, f is the frequency of the alternating E-field, ε is the dielectric permittivity, and V_i is the scalar potential of electrode i. The E-field $\boldsymbol{E_i}$ is calculated for each electrode from Equation (1b).

For a set of n different electrodes i, with amplitude settings v_i, all $\boldsymbol{E_i}$ can be superposed to obtain the total E-field E_{tot} as:

$$\boldsymbol{E_{tot}} = \sum_{i=1}^{n} \boldsymbol{E}\, v_i = \mathbf{Ev}. \tag{2}$$

The power loss density (P) produced by the total field can then be derived from:

$$P = \sigma \frac{|\boldsymbol{E_{tot}}|^2}{2} = \frac{\sigma}{2} \mathbf{v^H E}^H \mathbf{Ev} = \mathbf{v^H Pv}, \tag{3}$$

where **P** is an $n \times n$ matrix, and $\mathbf{E}^H$ and $\mathbf{v}^H$ are the Hermitian transpose of **E** and **v**, respectively.

For the E-field calculation (Figure 1 Item 3), the electric tissue properties are assigned according to the IT'IS database [37]. The electric properties of all used tissues, as well as those of the TBT applicator materials, are summarized in Table 1. All E-field and power calculations are performed in Sim4Life v6.2 (ZMT, Zurich, Switzerland).

Table 1. Electric and thermal properties of the applicator materials and the tissues used in the simulations.

Tissue	ρ (kg/m^3)	σ @27 MHz (S/m)	ε_r @27 MHz	c (J/kg/K)	k (W/m/K)	ω (ml/kg/min)
Applicator Dielectric [38,39]	1289	1×10^{-5}	2.4	712	0.084	-
Air [37]	1.164	0	1.0	1004	0.0273	-
Muscle [37]	1090.4	0.654	95.8	3421	0.495	40
Fat [37]	911	0.061	17.9	2348	0.211	33
Bone [37]	1908	0.052	21.8	1313	0.320	10
Prostate [37]	1045	0.838	120.1	3760	0.512	394
Rectum [37]	1045	0.654	95.8	3801	0.557	0
Urethra [37]	1102	0.375	88.8	3306	0.462	394
Bladder [37]	1086	0.276	31.5	3581	0.522	78

2.4. Temperature Calculation and Superpositioning

The temperature distribution (T) resulting from all electrodes can be calculated by solving the Pennes' bioheat equation [40,41]:

$$\rho c \frac{\partial T}{\partial t} = \nabla \cdot (k \nabla T) + \rho Q + P - \rho_b c_b \rho \omega (T - T_b) \tag{4}$$

where k is the thermal conductivity, c is the specific heat capacity, Q denotes the specific metabolic heat generation rate, and ω is the perfusion rate. ρ is the mass density of the medium. T_b, ρ_b, and c_b are the temperature, mass density, and specific heat capacity of blood, respectively. According to Das et al. [42], the temperature solution can be rewritten as:

$$T = \mathbf{v^H Tv} + T \tag{5}$$

where **T**, similar to **P** in (3), is an $n \times n$ matrix, and T_b is equal to the baseline temperature in the case of Dirichlet boundary conditions.

A fast optimization process is essential when applying simultaneous HDR-BT and IHT. To achieve faster temperature optimization, we use temperature superpositioning per electrode (Figure 1 Item 4), as proposed by Salgaonkar et al. for ultrasound-based IHT-TP [33]. In this method, all off-diagonal terms of **T** are neglected, reducing the complexity of the problem. With ΔT_i, the temperature increase resulting from the power loss density P_i, Equation (5) is simplified to:

$$T = \sum_{i=1}^{n} v_i^2 \Delta T + T_b \tag{6}$$

Under the above assumption (temperature superpositioning per electrode), the temperature T_i generated by each electrode i can be computed by solving the Pennes' bioheat Equa-

tion as in (4). The precomputed temperature distributions per electrode were calculated using a finite element method (FEM) solver in Sim4Life v6.2 (ZMT, Zurich, Switzerland).

2.5. HDR-BT Treatment Plan and Dose Calculation

The HDR-BT treatment planning protocol is defined using dose–volume metrics. The prescribed radiation dose (D_p) needs to be reached in at least 95% of the total target volume ($V_{100\%} \geq 95\%$). For the OAR, the dose in a particular volume x (D_x) is constrained to an organ-specific limit. The detailed HDR-BT treatment planning protocol is summarized in Table 2 and is based on [8].

Table 2. Fraction dose objectives and constraints of the clinical HDR-BT protocol.

Tissue	Criterion	Aim	Type
Prostate	$V_{100\%}$	≥95%	Objective
	$V_{150\%}$	<30%	Soft Constraint
	$V_{200\%}$	<8%	Soft Constraint
Urethra	$D_{0.1cc}$	<115%	Hard Constraint
Rectum	D_{1cc}	<75%	Hard Constraint
Bladder	D_{1cc}	<75%	Soft Constraint

The HDR-BT treatment plan (Figure 1 Item 5) is generated by expert radiotherapy technologists, based on inverse planning by simulated annealing [43] and manual finetuning, using the Oncentra® Brachy treatment planning software, and reviewed by a radiation oncologist. The HDR-BT treatment plan is based solely on the radiation dose generated by an HDR ^{192}Ir Flexisource, without considering the effect of the IHT. For the radiation dose calculation, a dose kernel based on the TG-43 standard is used [44].

2.6. Thermoradiobiological Modeling

To calculate the combined effect of the radiation and hyperthermia dose, thermoradiobiological modeling was performed (Figure 1 Item 6). The TDLQ model was applied [29]:

$$S(D,T) = \exp\left[-\alpha(T)\cdot D - \beta(T)\cdot D^2\right], \tag{7}$$

where *S(D,T)* is the surviving fraction of tissue when simultaneously exposed to a radiation dose D and a temperature T for 1 h, assuming that the parameters *α(T)* and *β(T)* are exponentially dependent on the temperature according to:

$$\alpha(T) = \alpha(37)\cdot exp\left[\frac{T-37}{T_{ref}-37}\cdot ln\left[\frac{\alpha\left(T_{ref}\right)}{\alpha(37)}\right]\right], \tag{8a}$$

$$\beta(T) = \beta(37)\cdot exp\left[\frac{T-37}{T_{ref}-37}\cdot ln\left[\frac{\beta\left(T_{ref}\right)}{\beta(37)}\right]\right], \tag{8b}$$

where T_{ref} is a reference temperature at which the $\alpha\left(T_{ref}\right)$ and $\beta\left(T_{ref}\right)$ have known values.

With this model, the equivalent dose received by a tissue, taking the thermal radiosensitization into account, is:

$$EQD_{ref} = \frac{\alpha(T)\cdot D + G\cdot\beta(T)\cdot D^2}{\alpha(37)+\beta(37)\cdot d_{ref}}, \tag{9}$$

where d_{ref} is the fraction dose to which the dose is normalized, and G is the Lea-Catcheside dose protraction factor, which is equal to 1 for a high dose rate source.

In our implementation, the equivalent dose is calculated normalized to the physical dose D. From Equations (8) and (9), this is calculated as:

$$EQD_{phys} = \frac{\frac{\alpha(37)}{\beta(37)} exp\left[\frac{T-37}{T_{ref}-37} \cdot ln\left[\frac{\alpha(T_{ref})}{\alpha(37)}\right]\right] \cdot D + exp\left[\frac{T-37}{T_{ref}-37} \cdot ln\left[\frac{\beta(T_{ref})}{\beta(37)}\right]\right] \cdot D^2}{\frac{\alpha(37)}{\beta(37)} + D} \quad (10)$$

where the values of the radiobiological parameter $\alpha/\beta = \alpha(37)/\beta(37)$, and the thermoradiobiological parameters $\alpha(T_{ref})/\alpha(37)$ and $\beta(T_{ref})/\beta(37)$ for a given temperature T_{ref} are needed for each tissue. The thermoradiobiological parameters for prostate tissue are assigned according to the in vitro data on the PC-3 and DU-145 prostate cancer cell lines in Pajonk et al. [16]. For normal tissues, there are no thermoradiobiological data available. Based on Overgaard [26], we can assume α and β parameters of normal tissue to have a similar thermal radiosensitization pattern as tumor tissue for the setting of simultaneous irradiation and hyperthermia; hence, we assigned the same $\alpha(T_{ref})/\alpha(37)$ and $\beta(T_{ref})/\beta(37)$ values to normal tissue. The radiobiological parameter α/β is conservatively set equal to 3 for all tissues at a normal temperature of 37 °C [45]. The values of all parameters are summarized in Table 3. Note that, in all following dose volume and dose coverage criteria in this article, dose is quantified in terms of EQD_{phys}, which is temperature-dependent in the case of TBT and equal to the physical dose, D, in the case of BT only.

Table 3. Thermoradiobiological parameters applied in this study, with T_{ref} = 43 °C.

Tissue	$\alpha(37)/\beta(37)$	$\alpha(43)/\alpha(37)$	$\beta(43)/\beta(37)$
Prostate	3		
PC-3 [16]		2.4	6.8
DU-145 [16]		0.8	1.8
Normal Tissue	3		

2.7. Thermoradiobiological Objective Function and Optimization Algorithm

For the optimization of the electrode amplitudes v_i in the TBT treatment, an equivalent physical dose (EQD_{phys}) based optimization algorithm is used (Figure 1 Item 8). The objectives are based on the criteria as reported in Table 2, combined with an overall upper temperature limit of T_{max} = 47.5 °C [20]. This is formulated in a minimization problem containing penalty functions PF_i for every violated constraint i, and objective scoring functions SF_j that return lower values for better performance for an objective j:

$$\Omega = W \sum_i PF_i + \sum_j SF_j \,. \quad (11)$$

The penalty functions PF_i are in the form of:

$$PF_i = \max[0, p_i(C - L_i)], \quad (12a)$$

where the values for C_i and L_i are according to Table 4 and the polarity factor p_i is +1 for low pass constraints and −1 for high pass constraints. The scoring functions SF_j are in the form of:

$$SF_i = -w_j|O_j - G_j| \,, \quad (12b)$$

where the values for O_i, G_j, and w_j are according to Table 4 (Figure 1 Item 7). The penalty weight factor W is set to a constant $W = 10^3$ for all constraints in order to ensure a high penalty for every constraint violation. The objective function Ω is minimized using a particle swarm optimization algorithm in MATLAB (MathWorks Inc., Natick, MA, USA).

2.8. Temperature Superpositioning Validation

While the temperature superpositioning method for fast temperature calculations has been validated for interstitial ultrasound power sources [33], we also perform a validation in our approach. To validate the accuracy of the temperature superpositioning method, we calculated a temperature distribution using the superpositioning method and we recalculated the temperature distribution resulting from the same power amplitudes using

the FEM solver. In this way, we investigated the assumption of Equation (4) that the off-diagonal terms in **T** not contributing significantly to the total temperature distribution is correct. The agreement between the two calculation methods was scored using three-dimensional γ-index analysis [46,47].

Table 4. Constraints and objectives applied in the objective function.

Constraints	Tissue	Criterion (C_i)	Limit (L_i)	Type
	Prostate	$V_{100\%}$	Value of BT-only	High pass
	Urethra	$D_{0.1cc}$	Value of BT-only	Low pass
	Rectum	D_{1cc}	Value of BT-only	Low pass
	Bladder	D_{1cc}	Value of BT-only	Low pass
	All	T_{max}	47.5 °C	Low pass
Objectives	**Tissue**	**Criterion (O_j)**	**Goal (G_j)**	**Weight (w_i)**
	Urethra	$D_{0.1cc}$	0	1
	Rectum	D_{1cc}	0	1
	Prostate	$V_{150\%}$	30% of volume	0.01

2.9. Implementation on Patient Data

To evaluate the proposed TBT treatment plan, we used data of 10 prostate cancer patients treated at our institution with HDR-BT monotherapy in two fractions of D_p = 13.5 Gy in a single day with a single implantation. For the first fraction, the patients were treated with a US-based HDR-BT treatment and, for the second fraction, they were treated with a CT-based HDR-BT treatment [35]. To validate the implementation of our treatment plan, we simulated a replacement for the second fraction by a TBT treatment and compared the resulting EQD_{phys} distribution to the original HDR-BT-only physical dose distribution by assuming that the TBT applicators are placed at the same position as the flexible 6F ProGuide afterloading needles (Elekta Brachytherapy Solutions, Veenendaal, The Netherlands).

The TBT treatment plan used a uniformly scaled-down version of the original HDR-BT dose distribution that had been clinically generated [35]. Different plans were generated using various combinations for the thermoradiobiological parameters $\alpha(43)/\alpha(37)$ and $\beta(43)/\beta(37)$, according to Table 3. The BT dose distributions were scaled from 70% to 95% of the original clinical dose. This process is illustrated in Figure 3.

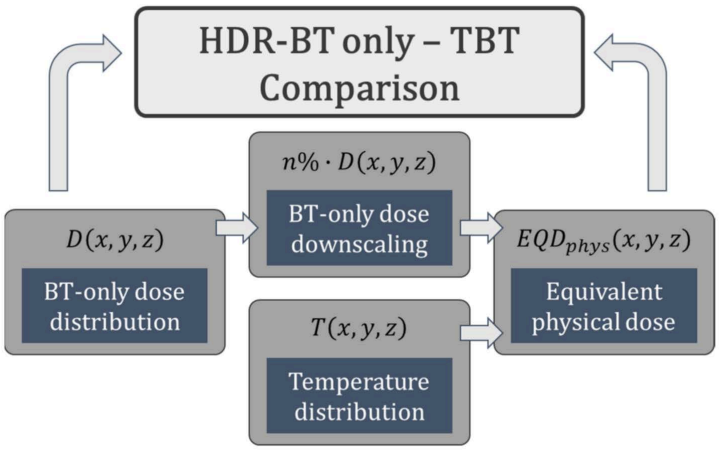

Figure 3. Flowchart illustrating how the TBT EQD_{phys} distribution is generated from and compared with the original BT-only dose distribution.

3. Results

3.1. Temperature Superpositioning Validation

The temperature distribution in a simulated patient with 18 applicators with given electrode amplitudes was calculated using both the superpositioning method (Figure 4a) and an FEM recalculation (Figure 4b). With the FEM-recalculated temperature as a reference, a γ-index analysis was performed. Applying 5%/0.5 mm dose difference and distance to agreement criteria, a passing rate >95% was observed, suggesting a good match to the reference (Figure 4c). As can be seen in Figure 4c, the highest gamma index values were positioned in the far-field of the temperature increase, where temperature values were low.

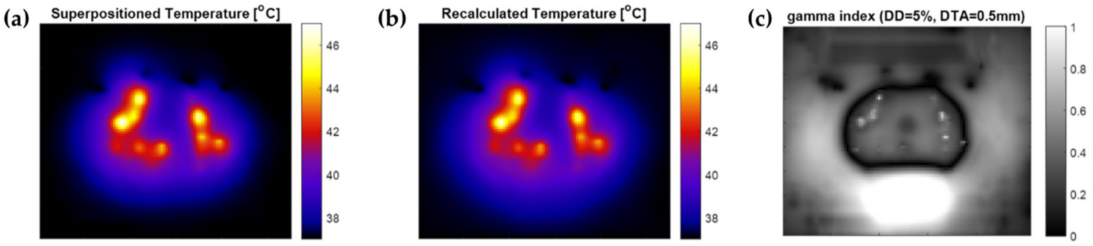

Figure 4. Comparison between superpositioned temperature calculation and FEM recalculation on the central axial slice in the prostate. (**a**) Temperature map using superpositioning of separate FEM calculations for each electrode. (**b**) Temperature map using a single FEM calculation for the same, combined, electrode settings. (**c**) γ-index map of the comparison.

3.2. Thermal Radiosensitization

To illustrate the thermal radiosensitization that is expected in prostate cancer cells, we applied the values of Table 3 to Equation (10) and visualized the results for different radiation doses and temperatures. How those values affect the EQD_{phys} dose resulting from a TBT treatment can be seen in Figure 5. As can be seen, there is a considerable difference in thermal radiosensitization between the PC-3 and DU-145 cell lines. Indicatively, the thermal enhancement caused by a 43 °C temperature in PC-3 is approximately threefold that of DU-145.

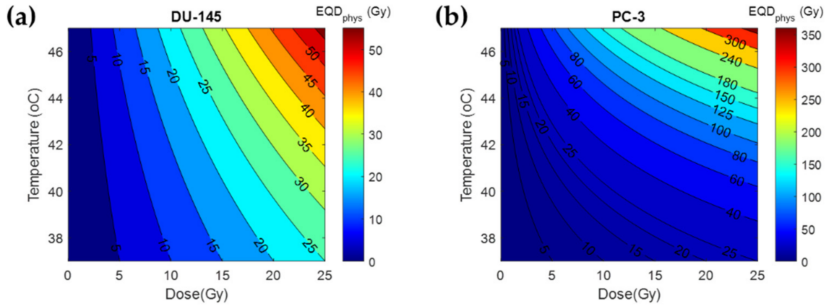

Figure 5. Isodose curves for the EQD_{phys} resulting from different combinations of physical dose and temperature for 1 h: (**a**) EQD_{phys} assuming DU-145 data; (**b**) EQD_{phys} assuming PC-3 data.

3.3. Treatment Planning Results

We optimized the temperature distribution for the 10 simulated patient plans for different scalings of the HDR-BT dose. Figure 6 shows the results for a single patient with an HDR-BT dose scaling of 80%. The $\alpha(43)/\alpha(37)$ and $\beta(43)/\beta(37)$ values are assumed equal to the average between DU-145 and PC-3 data, which gives $\alpha(43)/\alpha(37) = 1.6$ and $\beta(43)/\beta(37) = 4.3$. The EQD_{phys} volume histogram shows that the same target coverage is reached (96.6%), while $D_{0.1cc}$ for the urethra, and D_{1cc} for the rectum and bladder are reduced by 6.1%, 4.9%, and 8.2% of the prescribed dose, respectively. On the other hand, the $V_{150\%}$ and $V_{200\%}$ are higher by 12.1% and 12.4% of prostate volume, respectively.

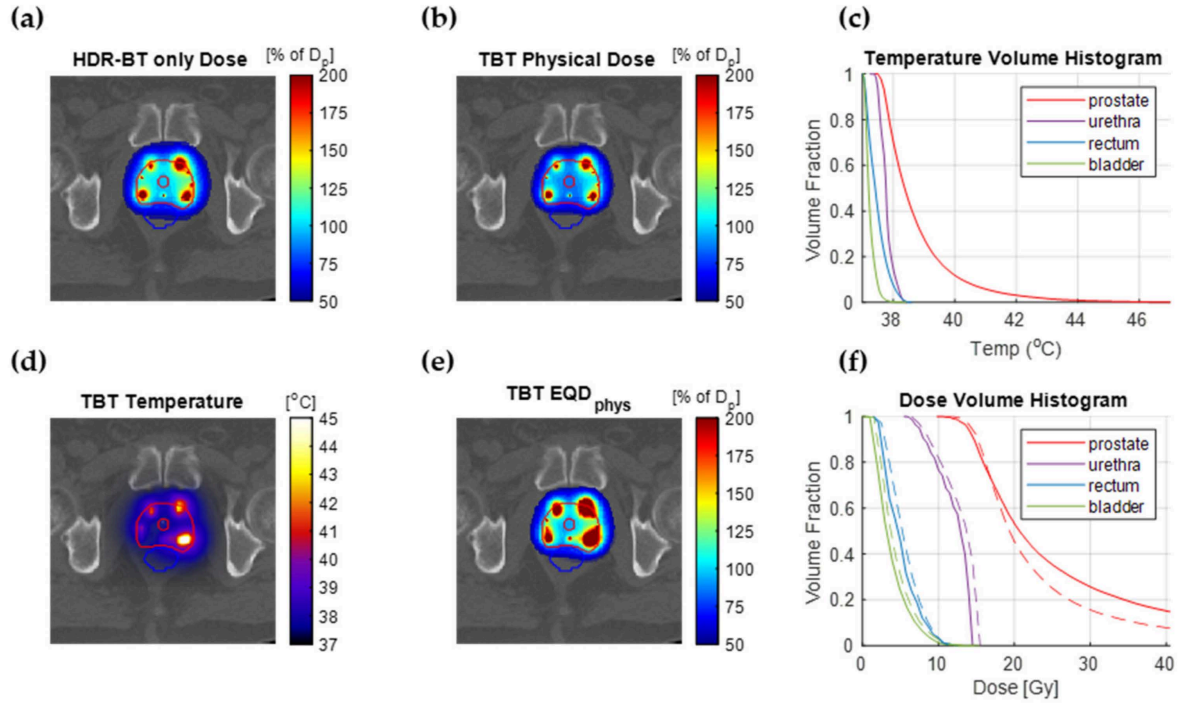

Figure 6. TBT TP results assuming thermoradiobiological parameters equal to the average between DU-145 and PC-3 data. (**a**) The original clinically applied HDR-BT dose fraction. (**b**) The applied TBT physical dose (80% of original). (**c**) Temperature volume histogram showing the temperature coverage in the prostate and OARs. (**d**) The temperature distribution calculated for the optimal TBT plan. (**e**) The TBT EQD_{phys} resulting from the combined treatment. (**f**) Dose volume histogram of the prostate and OARs for the HDR-BT-only dose (dashed line) and the TBT EQD_{phys} dose (solid line).

Figure 7 summarizes the results over all simulated patients (showing average values and standard deviations) for the prostate. From this figure, it can be seen that the required target coverage can be reached when using at least 80% of the original physical dose of the HDR-BT-only treatment (Figure 7a) for the less thermosensitive DU-145 cells. This result is valid for all three evaluated values of $\alpha(43)/\alpha(37)$ and $\beta(43)/\beta(37)$: PC-3, DU-145, and average. For radiosensitization according to the more thermosensitive PC-3 cells, this is as low as 70% of the original physical dose. It is evident that the addition of IHT contributes to considerably higher values for $V_{150\%}$ and $V_{200\%}$. This should be expected, since the IHT sources and HDR-BT sources irradiate from the same positions: the TBT applicator.

Figure 8 shows the T_{10}, T_{50}, and T_{90} values (temperature reached in at least 10%, 50%, and 90% of the total volume, respectively) over all simulated patients. It is evident that higher T_{10}, T_{50}, and T_{90} values are required for lower physical doses and for lower thermal sensitivity of the tumor. Furthermore, T_{50} and T_{90} values are mainly under the 39 °C value. This means that hyperthermia values are not needed in the whole prostate to reach the optimal EQD_{phys} distribution. On the other hand, the temperature is, as is the radiation dose, per definition, heterogeneous in the prostate.

For the OAR there are no data available on their sensitivity. Therefore, we evaluated the dose metrics for two extreme cases: assuming sensitization as high as in tumor tissue [26] and assuming no sensitization. The actual sensitization is expected to be somewhere in between the two extreme values. The OAR dose metrics reached with the different TBT plans are visualized in Figure 9. For all evaluated cases, the $D_{0.1cc}$ of the urethra, the D_{1cc} of the rectum, and the D_{1cc} of the bladder are lower with the TBT plan than with the HDR-BT-only plan (p-value < 0.001, paired two-sided Wilcoxon signed rank test).

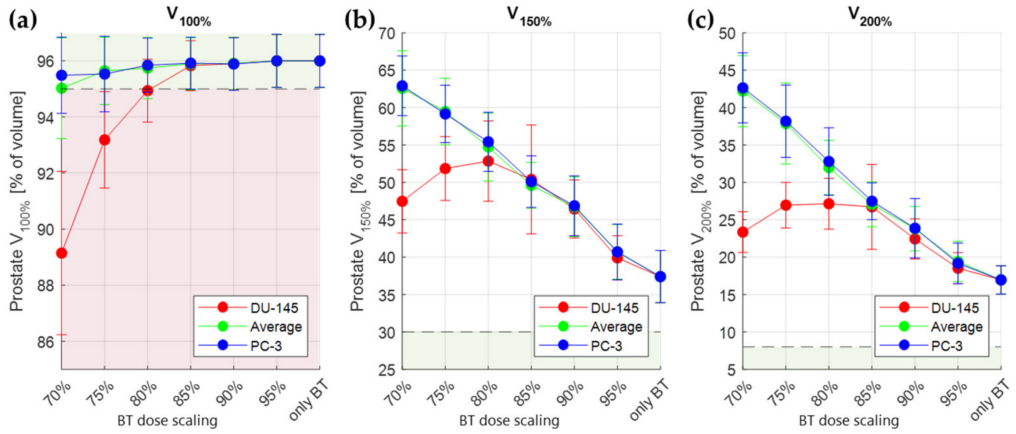

Figure 7. Average values (±standard deviation) over 10 simulated patients of TBT prostate $V_{100\%}$ (**a**), $V_{150\%}$ (**b**), and $V_{200\%}$ (**c**) for different scalings of the original HDR-BT dose. The different colors correspond to the plans generated based on different thermoradiotherapeutic values (red for DU-145, blue for PC-3, and green for the average between DU-145 and PC-3). It is evident that the original prostate coverage is met when the physical dose is scaled over 80% of the original value. The vertical bars correspond to standard deviation. The horizontal dashed lines correspond to the objective ($V_{100\%}$) and soft constraint ($V_{150\%}$ and $V_{200\%}$) limits. The green and red areas correspond to targeted and constrained values, respectively.

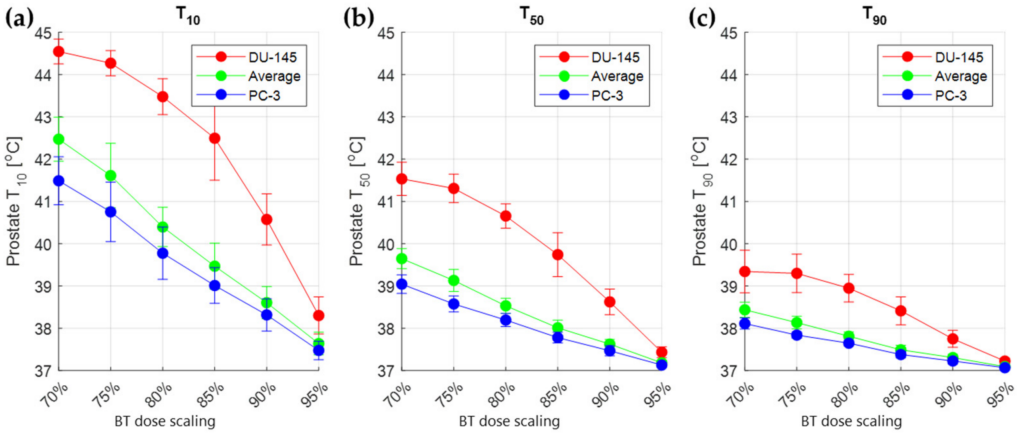

Figure 8. Average values (±standard deviation) over 10 simulated patients of the optimal TBT prostate T_{10} (**a**), T_{50} (**b**), and T_{90} (**c**) for different scalings of the original HDR-BT dose. The different colors correspond to the plans generated based on different thermoradiotherapeutic values (red for DU-145, blue for PC-3, and green for the average between DU-145 and PC-3). The vertical bars correspond to standard deviation.

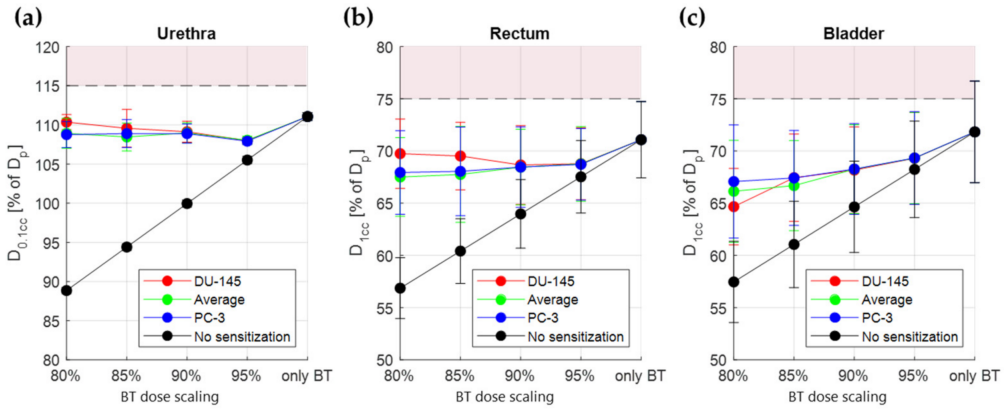

Figure 9. Average values (±standard deviation) over 10 simulated patients of the TBT TP parameters for different scaling of the original dose: urethra $D_{0.1cc}$ (**a**), rectum D_{1cc} (**b**), and bladder D_{1cc} (**c**). The different colors correspond to the plans generated based on different thermoradiotherapeutic values (red for DU-145, blue for PC-3, and green for the average between DU-145 and PC-3). The black line shows the lowest possible value, assuming no radiosensitization of the normal tissue. The horizontal dashed lines correspond to the constraint limit for each criterion. The red areas correspond to constrained values for each criterion.

4. Discussion

Extensive biological studies have indicated that hyperthermia is a potent sensitizer to radiotherapy, especially when applied simultaneously with the radiation dose [12,13]. To benefit from the high radiosensitization achieved in such a setting, both the thermal and radiation dose have to be focused sufficiently well to the target. In the TBT setting, both doses are administered from within the target region, which makes it the ideal method for simultaneous application. The highly localized deposition of both doses requires, however, good planning of the electrode amplitudes, dwell times, and dwell positions for good thermal and radiation coverage of the target and OAR sparing.

From a thermoradiobiological point of view, three-dimensional evaluation of combined radiotherapy and hyperthermia treatments is possible using the TDLQ model [29]. It is challenging to meet the set dose targets and constraints with the resulting EQD_{phys} without optimizing the temperature distribution according to those criteria. Given the high number of variables that need to be tuned, an automated method to optimize the temperature distribution is necessary for an optimal TBT treatment. Therefore, with the proposed optimization method, we can optimize the temperature on radiotherapeutic dose criteria.

To produce fast calculations of the temperature distribution, temperature superpositioning was used. We showed in our evaluation that this is a reasonable estimation of the temperature distribution, with a passing rate >95% for 5%/0.5 mm dose difference and distance to agreement criteria. It is important to note that the temperature calculation method showed the best results where high temperature elevations and consequently high radiosensitization were present (Figure 4), with the lower temperature regions mainly in the rectum showing less agreement with the single FEM temperature calculation. Therefore, with the current temperature calculation method, simulated rectum temperatures might not be reliable enough. For a more accurate estimation of the final temperature distribution, one could consider recalculating the final temperature distribution based on the optimal IHT-TP settings for evaluation purposes. Another option is to apply the method of Das et al. [42] (Equation (4)), although it would lead to slower optimizations due to the high number of electrodes producing an E-field.

We showed in our results (Figure 7) that the calculated TBT EQD_{phys} distribution can meet the prostate coverage $V_{100\%} \geq 95\%$ for different values of $\alpha(43)/\alpha(37)$ and $\beta(43)/\beta(37)$ with up to 20% decrease in physical dose (80% of original HDR-BT dose). For the required temperature elevations (Figure 8), it is evident that temperature homogeneity in the target

(Figure 6d) is not necessary to meet the prescribed target coverage. In the clinical feasibility study of the MECS applicator by van Vulpen et al. [48], it was noted that the observed high temperature gradients (T_{10} = 45.7 °C, T_{90} = 39.4 °C) were an undesired effect. By looking at the temperature distribution as a radiation dose sensitizer, we see that we can still reach significant improvements to the treatment, since only underdosed regions of the target are in need of a temperature increase.

Since there is no information available about the radiosensitization of normal tissues, we assumed in our optimization process a worst-case scenario of equal radiosensitization for normal and tumor tissue. With this assumption, we saw EQD_{phys} sparing for all three OAR (2.2 ± 1.7%, 2.6 ± 2.1%, and 4.2 ± 2.2% decrease for urethra $D_{0.1cc}$, rectum $D_{1cc,}$ and bladder D_{1cc}, respectively). In practice, we can expect a lower normal tissue radiosensitization than tumor tissue radiosensitization, especially since human prostate cancer cells are remarkably thermosensitive [15]. Therefore, we also evaluated the maximum potential decrease in the OAR by assuming no thermal radiosensitization in normal tissue (Figure 9). It is evident that OAR sparing can be significant in such a scenario (i.e., urethra $D_{0.1cc}$ as low as 90% of D_p). To draw definitive conclusions on the level of OAR sparing, the availability of thermoradiobiological data for normal tissues is an absolute requirement. Should the OAR sparing be insufficient, one can also investigate OAR cooling. Another option would be to investigate whether sequential TBT is beneficial. However, in sequential TBT the level of tumor radiosensitization is lower and the sequential procedure could prolong overall treatment time.

While OAR sparing can be expected, it is also evident from Figure 7 that the high target doses ($V_{150\%}$ and $V_{200\%}$) become even higher in the TBT setting. Namely, scaling down the physical dose increases the $V_{150\%}$ and $V_{200\%}$ to a saturation point where the $V_{100\%}$ target can be reached (for DU-145, this is visible at 80% target coverage in Figure 7). This effect is expected, given the fact that both modalities are delivered to the target from within the same applicator. Whether this is a negative effect or not can be debated. On the one hand, clinical treatment protocols strive to decrease extreme heterogeneity in the tumor by applying soft constraints on the high prostate doses, as is also carried out in the current study [6,49]. On the other hand, guidelines on prostate HDR-BT do not restrict high doses [10,11]. This can be explained by the fact that a saturation dose beyond which no further injury can occur likely exists in prostate brachytherapy [50,51].

In this study, we only optimize the temperature distribution based on the combined treatment. We expect that also optimizing the radiation dose distribution based on the combined effect has the potential to lead to more enhancement, i.e., better results, given the higher number of degrees of freedom. This additional optimization opportunity should, therefore, be considered in future research.

The TDLQ model is not complete in describing the combined effect of radiation and temperature elevation. The extended TDLQ model incorporating direct temperature-induced cytotoxicity has also been proposed and evaluated for cervical cancer cell lines [30]. There are currently not enough data to apply the same model for prostate cancer. However, in our application, where very high radiation fraction doses are applied, it can be presumed that most of the cell death is caused by radiation rather than temperature increase. In any case, should there be enough radiobiological data available, a more elaborate model could easily be applied to this algorithm as well.

In Figure 8, we showed that the calculated T_{10}, T_{50}, and T_{90} values needed for sufficient target coverage are, in some cases, lower than what is commonly regarded as adequate temperature elevation in hyperthermia treatments. These values are, however, set for an IHT treatment duration of 1 h. It is debatable whether temperatures under 39 °C can cause tumor radiosensitization at all [52]. One can, therefore, choose to normalize the length of the treatment to achieve the same thermal dose in, i.e., *CEM43* [12] or *AUC* [52]. This is also convenient in a simultaneous TBT treatment, since an HDR-BT treatment has a delivery time of approximately 10–20 min.

We have presented a method for automated IHT-TP optimization based on thermoradiotherapeutic criteria when IHT is used simultaneously with HDR-BT. We also showed that the results of the optimization are very dependent on the thermosensitivity of the tumor and normal tissue. With information on thermosensitivity of the involved tissues not yet available, the full potential use of this algorithm still needs to be determined. However, it can already serve as a promising tool for further development of IHT in combination with HDR-BT.

5. Conclusions

In this study, we presented a framework to optimize the temperature for simultaneous HDR-BT and IHT, based on the resulting EQD_{phys} of the combined treatment. This gives the opportunity of treatment planning on the same radiotherapeutic dose constraints and objectives as for HDR-BT only. We established that the fast calculation of the temperature distribution is accurate. Furthermore, on a sample of 10 patients, the calculated equivalent dose distribution predicts a favorable reduction in the dose in OARs. At the same time, the target dose coverage remains at the same level as prescribed in the standard protocol, while the high-dose regions ($V_{150\%}$ and $V_{200\%}$) get considerably higher values. While this framework offers a valuable tool for simultaneous thermobrachytherapy treatment plan optimization, further research on the biological effects of both heat and radiation is needed to confirm the clinical relevance of a simultaneous thermobrachytherapy treatment.

Author Contributions: Conceptualization, I.A., G.C.v.R., I.-K.K.K.-D., R.M.C.M. and M.E.M.C.C.; methodology, I.A.; software, I.A.; validation, I.A., R.M.C.M. and I.-K.K.K.-D.; formal analysis, I.A.; investigation, I.A.; resources, G.C.v.R., I.-K.K.K.-D. and M.E.M.C.C.; writing—original draft preparation, I.A.; writing—review and editing, G.C.v.R., R.M.C.M., M.E.M.C.C. and I.-K.K.K.-D.; visualization, I.A.; supervision, G.C.v.R., M.E.M.C.C., R.M.C.M. and I.-K.K.K.-D.; project administration, G.C.v.R.; funding acquisition, G.C.v.R. All authors have read and agreed to the published version of the manuscript.

Funding: This research was funded by Elekta, grant number 106932, task 4.

Institutional Review Board Statement: The study was conducted according to the guidelines of the Declaration of Helsinki, and approved by the Institutional Review Board (or Ethics Committee) of Erasmus Medical Center Rotterdam (METC 2018-1711, date of approval 14-01-2019).

Informed Consent Statement: Informed consent was obtained from all subjects involved in the study.

Data Availability Statement: The data presented in this study can be made available upon request to the corresponding author.

Conflicts of Interest: The authors declare no conflict of interest. The funders had no role in the design of the study; in the collection, analyses, or interpretation of data; in the writing of the manuscript, or in the decision to publish the results.

References

1. Litwin, M.S.; Tan, H.-J. The Diagnosis and Treatment of Prostate Cancer: A Review. *JAMA* **2017**, *317*, 2532–2542. [CrossRef] [PubMed]
2. Miralbell, R.; Roberts, S.A.; Zubizarreta, E.; Hendry, J.H. Dose-Fractionation Sensitivity of Prostate Cancer Deduced from Radiotherapy Outcomes of 5,969 Patients in Seven International Institutional Datasets: α/β = 1.4 (0.9–2.2) Gy. *Int. J. Radiat. Oncol. Biol. Phys.* **2012**, *82*, e17–e24. [CrossRef] [PubMed]
3. Gocho, T.; Hori, M.; Fukushima, Y.; Someya, M.; Kitagawa, M.; Hasegawa, T.; Tsuchiya, T.; Hareyama, M.; Takagi, M.; Hashimoto, K. Evaluation of the Urethral α/β Ratio and Tissue Repair Half-Time for Iodine-125 Prostate Brachytherapy with or without Supplemental External Beam Radiotherapy. *Brachytherapy* **2020**, *19*, 290–297. [CrossRef] [PubMed]
4. Brand, D.H.; Brüningk, S.C.; Wilkins, A.; Fernandez, K.; Naismith, O.; Gao, A.; Syndikus, I.; Dearnaley, D.P.; Tree, A.C.; van As, N. Estimates of Alpha/Beta (α/β) Ratios for Individual Late Rectal Toxicity Endpoints: An Analysis of the CHHiP Trial. *Int. J. Radiat. Oncol. Biol. Phys.* **2021**, *110*, 596–608. [CrossRef] [PubMed]
5. Morton, G.C. High-Dose-Rate Brachytherapy Boost for Prostate Cancer: Rationale and Technique. *J. Contemp. Brachyther.* **2014**, *6*, 323. [CrossRef] [PubMed]

6. Tselis, N.; Hoskin, P.; Baltas, D.; Strnad, V.; Zamboglou, N.; Rödel, C.; Chatzikonstantinou, G. High Dose Rate Brachytherapy as Monotherapy for Localised Prostate Cancer: Review of the Current Status. *Clin. Oncol. R. Coll. Radiol.* **2017**, *29*, 401–411. [CrossRef] [PubMed]
7. Hoskin, P.; Rojas, A.; Lowe, G.; Bryant, L.; Ostler, P.; Hughes, R.; Milner, J.; Cladd, H. High-Dose-Rate Brachytherapy Alone for Localized Prostate Cancer in Patients at Moderate or High Risk of Biochemical Recurrence. *Int. J. Radiat. Oncol.* **2012**, *82*, 1376–1384. [CrossRef]
8. Nagore, G.; Guerra, J.L.L.; Krumina, E.; Lagos, M.; Ovalles, B.; Miró, A.; Beltran, L.; Gómez, E.; Praena-Fernandez, J.M.; del Campo, E.R.; et al. High Dose Rate Brachytherapy for Prostate Cancer: A Prospective Toxicity Evaluation of a One Day Schedule Including Two 13.5 Gy Fractions. *Radiother. Oncol.* **2018**, *127*, 219–224. [CrossRef]
9. Aluwini, S.; Busser, W.M.; Alemayehu, W.G.; Boormans, J.L.; Kirkels, W.J.; Jansen, P.P.; Praag, J.O.; Bangma, C.H.; Kolkman-Deurloo, I.-K.K. Toxicity and Quality of Life after High-Dose-Rate Brachytherapy as Monotherapy for Low- and Intermediate-Risk Prostate Cancer. *Radiother. Oncol.* **2015**, *117*, 252–257. [CrossRef]
10. Hoskin, P.; Colombo, A.; Henry, A.; Niehoff, P.; Hellebust, T.P.; Siebert, F.-A.; Kovacs, G. GEC/ESTRO Recommendations on High Dose Rate Afterloading Brachytherapy for Localised Prostate Cancer: An Update. *Radiother. Oncol.* **2013**, *107*, 325–332. [CrossRef]
11. Yamada, Y.; Rogers, L.; Demanes, D.J.; Morton, G.; Prestidge, B.R.; Pouliot, J.; Cohen, G.; Zaider, M.; Ghilezan, M.; Hsu, I.-C. American Brachytherapy Society consensus guidelines for high-dose-rate prostate brachytherapy. *Brachytherapy* **2012**, *11*, 20–32. [CrossRef]
12. Van Rhoon, G.C. Is CEM43 Still a Relevant Thermal Dose Parameter for Hyperthermia Treatment Monitoring? *Int. J. Hyperth.* **2016**, *32*, 50–62. [CrossRef]
13. Horsman, M.R.; Overgaard, J. Hyperthermia: A Potent Enhancer of Radiotherapy. *Clin. Oncol.* **2007**, *19*, 418–426. [CrossRef]
14. Datta, N.R.; Bodis, S. Hyperthermia with Radiotherapy Reduces Tumour Alpha/Beta: Insights from Trials of Thermoradiotherapy vs. Radiotherapy Alone. *Radiother. Oncol.* **2019**, *138*, 1–8. [CrossRef]
15. Ryu, S.; Brown, S.L.; Kim, S.-H.; Khil, M.S.; Kim, J.H. Preferential Radiosensitization of Human Prostatic Carcinoma Cells by Mild Hyperthermia. *Int. J. Radiat. Oncol.* **1996**, *34*, 133–138. [CrossRef]
16. Pajonk, F.; Van Ophoven, A.; McBride, W.H. Hyperthermia-Induced Proteasome Inhibition and Loss of Androgen Receptor Expression in Human Prostate Cancer Cells. *Cancer Res.* **2005**, *65*, 4836–4843. [CrossRef]
17. Rajaee, Z.; Khoei, S.; Mahdavi, S.R.; Ebrahimi, M.; Shirvalilou, S.; Mahdavian, A. Evaluation of the Effect of Hyperthermia and Electron Radiation on Prostate Cancer Stem Cells. *Radiat. Environ. Biophys.* **2018**, *57*, 133–142. [CrossRef]
18. Elming, P.B.; Sørensen, B.S.; Oei, A.L.; Franken, N.A.P.; Crezee, J.; Overgaard, J.; Horsman, M.R. Hyperthermia: The Optimal Treatment to Overcome Radiation Resistant Hypoxia. *Cancers* **2019**, *11*, 60. [CrossRef]
19. Morton, G.C.; Hoskin, P.J. Single Fraction High-Dose-Rate Brachytherapy: Too good to Be True? *Int. J. Radiat. Oncol. Biol. Phys.* **2019**, *104*, 1054–1056. [CrossRef]
20. Dobšíček Trefná, H.; Schmidt, M.; van Rhoon, G.C.; Kok, H.P.; Gordeyev, S.S.; Lamprecht, U.; Marder, D.; Nadobny, J.; Ghadjar, P.; Abdel-Rahman, S.; et al. Quality Assurance Guidelines for Interstitial Hyperthermia. *Int. J. Hyperth.* **2019**, *36*, 276–293. [CrossRef]
21. Prionas, S.D.; Kapp, D.S.; Goffinet, D.R.; Ben-Yosef, R.; Fessenden, P.; Bagshaw, M.A. Thermometry of Interstitial Hyperthermia Given as an Adjuvant to Brachytherapy for the Treatment of Carcinoma of the Prostate. *Int. J. Radiat. Oncol.* **1994**, *28*, 151–162. [CrossRef]
22. Williams, V.L.; Puthawala, A.; Phan, T.P.; Sharma, A.; Syed, A.N. Interstitial Hyperthermia during HDR Brachytherapy Monotherapy for Treatment of Early Stage Prostate Cancer with Benign Prostate Hyperplasia (BPH). *Brachytherapy* **2007**, *6*, 86. [CrossRef]
23. Kukiełka, A.; Hetnał, M.; Dąbrowski, T.; Walasek, T.; Brandys, P.; Nahajowski, D.; Kudzia, R.; Dybek, D.; Reinfuss, M. Salvage Prostate HDR Brachytherapy Combined with Interstitial Hyperthermia for Local Recurrence after Radiation Therapy Failure. *Strahlenther. Onkol.* **2013**, *190*, 165–170. [CrossRef]
24. Mei, X.; Ten Cate, R.; Van Leeuwen, C.M.; Rodermond, H.M.; De Leeuw, L.; Dimitrakopoulou, D.; Stalpers, L.J.A.; Crezee, J.; Kok, H.P.; Franken, N.A.P.; et al. Radiosensitization by Hyperthermia: The Effects of Temperature, Sequence, and Time Interval in Cervical Cell Lines. *Cancers* **2020**, *12*, 582. [CrossRef]
25. Androulakis, I.; Mestrom, R.M.C.; Christianen, M.E.M.C.; Kolkman-Deurloo, I.-K.K.; van Rhoon, G.C. Design of the Novel ThermoBrachy Applicators Enabling Simultaneous Interstitial Hyperthermia and High Dose Rate Brachytherapy. *Int. J. Hyperth.* **2021**, *38*, 1660–1671. [CrossRef]
26. Overgaard, J. Simultaneous and Sequential Hyperthermia and Radiation Treatment of an Experimental Tumor and Its Surrounding Normal Tissue in Vivo. *Int. J. Radiat. Oncol.* **1980**, *6*, 1507–1517. [CrossRef]
27. Overgaard, J. The Heat Is (still) on—The Past and Future of Hyperthermic Radiation Oncology. *Radiother. Oncol.* **2013**, *109*, 185–187. [CrossRef]
28. Kok, H.P.; Crezee, J.; Franken, N.; Stalpers, L.J.; Barendsen, G.W.; Bel, A. Quantifying the Combined Effect of Radiation Therapy and Hyperthermia in Terms of Equivalent Dose Distributions. *Int. J. Radiat. Oncol.* **2014**, *88*, 739–745. [CrossRef]
29. Van Leeuwen, C.M.; Crezee, J.; Oei, A.L.; Franken, N.A.P.; Stalpers, L.J.A.; Bel, A.; Kok, H.P. 3D Radiobiological Evaluation of Combined Radiotherapy and Hyperthermia Treatments. *Int. J. Hyperth.* **2016**, *33*, 160–169. [CrossRef]
30. Van Leeuwen, C.M.; Oei, A.L.; Cate, R.T.; Franken, N.A.P.; Bel, A.; Stalpers, L.J.A.; Crezee, J.; Kok, H.P. Measurement and Analysis of the Impact of Time-Interval, Temperature and Radiation Dose on Tumour Cell Survival and Its Application in Thermoradiotherapy Plan Evaluation. *Int. J. Hyperth.* **2017**, *34*, 30–38. [CrossRef]

31. De Mendoza, A.M.; Michlíková, S.; Berger, J.; Karschau, J.; Kunz-Schughart, L.A.; McLeod, D.D. Mathematical Model for the Thermal Enhancement of Radiation Response: Thermodynamic Approach. *Sci. Rep.* **2021**, *11*, 5503. [CrossRef] [PubMed]
32. Chen, X.; Diederich, C.; Wootton, J.H.; Pouliot, J.; Hsu, I.-C. Optimisation-Based Thermal Treatment Planning for Catheter-Based Ultrasound Hyperthermia. *Int. J. Hyperth.* **2010**, *26*, 39–55. [CrossRef] [PubMed]
33. Salgaonkar, V.A.; Prakash, P.; Diederich, C.J. Temperature Superposition for Fast Computation of 3D Temperature Distributions during Optimization and Planning of Interstitial Ultrasound Hyperthermia Treatments. *Int. J. Hyperth.* **2012**, *28*, 235–249. [CrossRef] [PubMed]
34. Kok, H.P.; Kotte, A.N.T.J.; Crezee, J. Planning, Optimisation and Evaluation of Hyperthermia Treatments. *Int. J. Hyperth.* **2017**, *33*, 593–607. [CrossRef]
35. Androulakis, I.; Mestrom, R.M.C.; Christianen, M.E.M.C.; Kolkman-Deurloo, I.-K.K.; van Rhoon, G.C. Simultaneous Thermo-Brachytherapy: Electromagnetic Simulation Methods for Fast and Accurate Adaptive Treatment Planning. *Sensors* **2022**, *22*, 1328. [CrossRef]
36. Haus, H.A.; Melcher, J.R. *Electromagnetic Fields and Energy*; Prentice Hall Englewood Cliffs: Hoboken, NJ, USA, 1989; Volume 107.
37. Hasgall, P.A.; Di Gennaro, F.; Baumgartner, C.; Neufeld, E.; Lloyd, B.; Gosselin, M.C.; Payne, D.; Klingenböck, A.; Kuster, N. *IT'IS Database for Thermal and Electromagnetic Parameters of Biological Tissues*; Version 4.0; IT'IS Foundation: Zürich, Switzerland, 2018.
38. Khawaji, I.H.; Chindam, C.; Awadelkarim, O.O.; Lakhtakia, A. Dielectric Properties of and Charge Transport in Columnar Microfibrous Thin Films of Parylene C. *IEEE Trans. Electron. Devices* **2017**, *64*, 3360–3367. [CrossRef]
39. Kahouli, A.; Sylvestre, A.; Jomni, F.; Yangui, B.; Legrand, J. Experimental and Theoretical Study of AC Electrical Conduction Mechanisms of Semicrystalline Parylene C Thin Films. *J. Phys. Chem. A* **2012**, *116*, 1051–1058. [CrossRef]
40. Pennes, H.H. Analysis of Tissue and Arterial Blood Temperatures in the Resting Human Forearm. *J. Appl. Physiol.* **1948**, *1*, 93–122. [CrossRef]
41. Wissler, E.H. Pennes' 1948 Paper Revisited. *J. Appl. Physiol.* **1998**, *85*, 35–41. [CrossRef]
42. Das, S.K.; Clegg, S.T.; Samulski, T.V. Computational Techniques for Fast Hyperthermia Temperature Optimization. *Med. Phys.* **1999**, *26*, 319–328. [CrossRef]
43. Lessard, E.; Pouliot, J. Inverse Planning Anatomy-Based Dose Optimization for HDR-Brachytherapy of the Prostate Using Fast Simulated Annealing Algorithm and Dedicated Objective Function. *Med. Phys.* **2001**, *28*, 773–779. [CrossRef]
44. Perez-Calatayud, J.; Ballester, F.; Das, R.K.; DeWerd, L.A.; Ibbott, G.S.; Meigooni, A.S.; Ouhib, Z.; Rivard, M.J.; Sloboda, R.S.; Williamson, J.F. Dose Calculation for Photon-Emitting Brachytherapy Sources with Average Energy Higher than 50 keV: Report of the AAPM and ESTRO. *Med. Phys.* **2012**, *39*, 2904–2929. [CrossRef]
45. Roos, M.; Kolkman-Deurloo, I.-K.; De Pan, C.; Aluwini, S. Single Fraction HDR Brachytherapy as Monotherapy in Patients with Prostate Cancer: What Is the Optimal Dose Level? *Brachytherapy* **2016**, *15*, S167–S168. [CrossRef]
46. Low, D.A.; Harms, W.B.; Mutic, S.; Purdy, J.A. A Technique for the Quantitative Evaluation of Dose Distributions. *Med. Phys.* **1998**, *25*, 656–661. [CrossRef]
47. De Bruijne, M.; Samaras, T.; Chavannes, N.; van Rhoon, G.C. Quantitative Validation of the 3D SAR Profile of Hyperthermia Applicators Using the Gamma Method. *Phys. Med. Biol.* **2007**, *52*, 3075. [CrossRef]
48. Van Vulpen, M.; Raaymakers, B.W.; Lagendijk, J.J.W.; Crezee, J.; Leeuw, A.A.C.D.; Van Moorselaar, J.R.A.; Ligtvoet, C.M.; Battermann, J.J. Three-Dimensional Controlled Interstitial Hyperthermia Combined with Radiotherapy for Locally Advanced Prostate Carcinoma—A Feasibility Study. *Int. J. Radiat. Oncol.* **2002**, *53*, 116–126. [CrossRef]
49. Christianen, M.; De Vries, K.; Jansen, P.; Luthart, L.; Kolkman-Deurloo, I.; Nout, R. PO-0244 HDR Brachytherapy Monotherapy with 2 × 13.5 Gy for Localized Prostate Cancer: Short Term Follow Up. *Radiother. Oncol.* **2021**, *158*, S203–S204. [CrossRef]
50. Ling, C.; Roy, J.; Sahoo, N.; Wallner, K.; Anderson, L. Quantifying the Effect of Dose Inhomogeneity in Brachytherapy: Application to Permanent Prostatic Implant with 125I Seeds. *Int. J. Radiat. Oncol.* **1994**, *28*, 971–977. [CrossRef]
51. Fatyga, M.; Williamson, J.F.; Dogan, N.; Todor, D.; Siebers, J.V.; George, R.; Barani, I.; Hagan, M. A Comparison of HDR BrachyTherapy and IMRT Techniques for Dose Escalation in Prostate Cancer: A Radiobiological Modeling Study. *Med. Phys.* **2009**, *36*, 3995–4006. [CrossRef]
52. Datta, N.R.; Marder, D.; Datta, S.; Meister, A.; Puric, E.; Stutz, E.; Rogers, S.; Eberle, B.; Timm, O.; Staruch, M.; et al. Quantification of Thermal Dose in Moderate Clinical Hyperthermia with Radiotherapy: A Relook Using Temperature—Time Area under the Curve (AUC). *Int. J. Hyperth.* **2021**, *38*, 296–307. [CrossRef]